

Distances to Populous Clusters in the LMC via the K-band Luminosity of the Red Clump

Aaron J. Grocholski¹, Ata Sarajedini

*Department of Astronomy, University of Florida, P.O. Box 112055, Gainesville, FL 32611;
 aaron@astro.ufl.edu, ata@astro.ufl.edu*

Knut A. G. Olsen

*Cerro Tololo Inter-American Observatory, National Optical Astronomy Observatory,
 Casilla 603, La Serena, Chile; kolsen@noao.edu*

Glenn P. Tiede

*Department of Physics and Astronomy, Bowling Green State University, Bowling Green,
 OH, 43403; gptiede@bgnet.bgsu.edu*

and

Conor L. Mancone

*Department of Astronomy, University of Florida, P.O. Box 112055, Gainesville, FL 32611;
 cmancone@astro.ufl.edu*

ABSTRACT

We present results from a study of the distances and distribution of a sample of intermediate-age clusters in the Large Magellanic Cloud. Using deep near-infrared photometry obtained with ISPI on the CTIO 4m, we have measured the apparent K -band magnitude of the core helium burning red clump stars in 17 LMC clusters. We combine cluster ages and metallicities with the work of Grocholski & Sarajedini to predict each cluster's absolute K -band red clump magnitude, and thereby calculate absolute cluster distances. An analysis of these data shows that the cluster distribution is in good agreement with the thick, inclined disk geometry of the LMC, as defined by its field stars. We also find that the old globular clusters follow the same distribution, suggesting that the

¹Visiting Astronomer, Cerro Tololo Inter-American Observatory, National Optical Astronomy Observatory, which is operated by the Association of Universities for Research in Astronomy (AURA), Inc., under cooperative agreement with the National Science Foundation.

LMC’s disk formed at about the same time as the globular clusters, ~ 13 Gyr ago. Finally, we have used our cluster distances in conjunction with the disk geometry to calculate the distance to the LMC center, for which we find $(m - M)_0 = 18.40 \pm 0.04_{ran} \pm 0.08_{sys}$, or $D_0 = 47.9 \pm 0.9 \pm 1.8$ kpc.

Subject headings: Magellanic Clouds — galaxies:star clusters — galaxies:distances

1. Introduction

Interactions and merger events can dominate the formation histories of galaxies, both large and small, at high and low redshift (Abraham 1999; Schweizer 1999) and the Milky Way (MW) and its satellite galaxies are an excellent example of this. The Large Magellanic Cloud (LMC) is a nearby satellite galaxy that is dynamically active; it exhibits many epochs of star formation (including current star formation) while also suffering from tidal interactions with the Small Magellanic Cloud (SMC) and the MW. Given its proximity, stellar populations in the LMC are easily resolved, allowing us to obtain information such as ages, chemical abundances, kinematics and distances to individual stars. Thus, the LMC offers us an excellent local laboratory in which to study the effects of gravitational forces on the evolution of a satellite galaxy.

Traditionally, the LMC has been treated as a planar galaxy that, despite its proximity, can be assumed to lie at a single distance from us. This is in spite of the fact that, using distances to field Cepheid variables, Caldwell & Coulson (1986) first showed that the disk of the LMC is inclined with respect to the sky. More recent studies of field stars have confirmed this finding. For example, van der Marel & Cioni (2001) combined near infrared photometry from the Deep Near-Infrared Southern Sky Survey (DENIS) and the Two Micron All-Sky Survey (2MASS) to study the distribution of field stars in the LMC out to a radius of $\sim 7^\circ$. Using both the tip of the red giant branch (RGB) and asymptotic giant branch as relative distance indicators, they found an *I*-band peak-to-peak sinusoidal brightness variation of ~ 0.25 mag that changes as a function of position angle on the sky, with stars in the northeast portion of the LMC brighter than stars in the southwest. Attributing this variation in brightness to a difference in distance, they calculated an inclination of $i = 34.7 \pm 6.2$ for the disk of the LMC (where 0° is face on) and the line of nodes position angle (the intersection of the plane of the galaxy with the plane of the sky) of $\Theta = 122.5 \pm 8.3$. In an approach similar to van der Marel & Cioni (2001), Olsen & Salyk (2002) use the apparent *I*-band magnitude of core helium burning red clump (RC) stars to explore the structure of the disk. Calculating relative distances for 50 fields spread across a $6^\circ \times 6^\circ$ area of the LMC, they find $i = 35.8 \pm 2.4$, in agreement with the van der Marel & Cioni (2001) result, and

$\Theta = 145^\circ \pm 4^\circ$. In addition to the inclination, the LMC’s geometry becomes even more complex when we consider that its disk ($v/\sigma = 2.9 \pm 0.9$) is thicker than the MW’s thick disk ($v/\sigma \approx 3.9$, van der Marel et al. 2002) and that the disk is flared (Alves & Nelson 2000) and also possibly warped (Olsen & Salyk 2002; Nikolaev et al. 2004) as a result of interactions with the SMC and MW. Even with all of the knowledge of the LMC’s structure from field star studies, the spatial distribution of populous clusters in the LMC remains relatively unexplored. Schommer et al. (1992, see also Grocholski et al. 2006) showed that the LMC clusters have disk-like kinematics, however, only recently has a planar geometry been illustrated for the LMC cluster system (Kerber et al. 2006).

Distances to stellar populations in the LMC have been calculated using a variety of standard candles, including the period-luminosity (P-L) relation of Cepheid variables (e.g., Macri et al. 2006; Gieren et al. 1998), the mean absolute magnitude-metallicity relationship for RR Lyraes (e.g., Walker 1985), and color magnitude diagram (CMD) features like the tip of the RGB (e.g., Cioni et al. 2000), RC stars (e.g., Udalski 2000; Sarajedini et al. 2002), or main sequence turn off (MSTO; Kerber et al. 2006). One standard candle that has yet to be fully exploited, and is geared toward studying clusters, is the K -band luminosity of the RC. In their work, Grocholski & Sarajedini (2002, hereafter GS02) use 2MASS JK_S photometry of 14 Galactic open clusters that possess internally consistent ages, metallicities, and MSTO fitting distances to calibrate the absolute K -band magnitude of the RC (M_K^{RC}) as a function of age and metallicity. An important result from their study is that, while variations in the RC brightness are smaller in the K -band than what is seen in the V - or I -bands, M_K^{RC} varies as a function of both age and metallicity and, for young ages ($\lesssim 3$ Gyr), M_K^{RC} can vary by up to a magnitude. Therefore, knowledge of the abundances *and* ages of RC stars, something that can only be unequivocally gleaned from clusters, is necessary to properly employ the RC as a standard candle. Since this method provides an absolute distance, its application allows the determination of both the spatial distribution of clusters and the distance to the LMC.

The distance to the LMC has been of considerable interest in recent years, largely due to its use as the zeropoint for the extragalactic distance scale. The HST Key Project to determine H_0 (see Freedman et al. 2001 for final results on the project) used a sample of Cepheid variables in the LMC, along with an adopted distance of $(m - M)_0 = 18.5 \pm 0.1$ (Madore & Freedman 1991), to define the fiducial Cepheid P-L relation. Freedman et al. (2001) then used this new P-L relation to calculate distances to a large number of galaxies, thereby allowing the calibration of secondary standard candles (Type Ia and Type II supernovae, Tully-Fisher relation, surface brightness fluctuations, fundamental plane) that lie further up the extragalactic distance ladder. Thus, the accuracy of their value of $H_0 = 72 \pm 8$ $\text{km s}^{-1} \text{ Mpc}^{-1}$ is ultimately determined by the accuracy of the distance to the LMC; it turns

out that the distance error constitutes 6.5% of their 9% error budget. Their adopted distance, however, was based on previously published distances and, until recently, there have been rather large discrepancies between different methods and sometimes even among distances calculated using the same method (particularly with optical photometry of the RC). In general, the LMC distances can be split up into a “long” distance of $\sim 18.5\text{--}18.7$ mag, usually found with Population I indicators, and a “short” distance of ~ 18.3 mag, calculated primarily from RR Lyrae variables. Clementini et al. (2003) review the LMC distances and methods in detail and find that the long and short distance scales can be reconciled, at least to within the errors, with improved photometry and/or reddening estimates. From the distances they have collected (and corrected), Clementini et al. (2003) find a mean LMC distance of $(m - M)_0 = 18.515 \pm 0.085$, in good agreement with the value adopted by Freedman et al. (2001).

In an effort to determine the spatial distribution of the LMC cluster system and improve the accuracy of the distance to the LMC, we apply the approach of GS02 to calculating absolute distances to 17 populous clusters in the LMC. Cluster distances, combined with the geometry of the cluster system allow us to determine an accurate distance to the center of the LMC. In §2 we discuss the near-infrared data acquisition, reduction, and photometry. The cluster ages and abundances necessary for accurately determining M_K^{RC} are presented in §3 and in §4 we calculate K_{RC} and M_K^{RC} for our cluster sample. Finally, in §5, cluster distances and the distance to the center of the LMC are given, with a comparison to selected previous works in §6. Our results are summarized in §7.

2. Data

2.1. Observations

We have obtained near infrared images of a sample of populous LMC clusters over the course of six nights (20-22 January 2003 and 06-08 February 2004) at the Cerro Tololo Inter-America Observatory Blanco 4m telescope. All data were taken with the Infrared Side Port Imager (ISPI), which utilizes a 2048×2048 HAWAII 2 HgCdTe array. In the f/8 configuration, ISPI has a field of view of $\sim 10' \times 10'$ with a plate scale of $\sim 0''.33 \text{ pixel}^{-1}$. At the time of our observations, ISPI was equipped with J ($1.25 \mu\text{m}$), H ($1.64 \mu\text{m}$), and K' ($2.12 \mu\text{m}$) filters on loan from Gemini and all clusters were imaged in the J - and K' -bands with about half of the clusters also having H -band data. Average seeing for all six nights was $\sim 1.2''$.

Each cluster was observed with a nine-point dither pattern, centered on the cluster, with

dither offsets ranging between $30''$ and $120''$, depending on the size and density of the target. Total exposure time in each band was as follows: J - 540s; H - 846s; K' - 846s. For the first run, H - and K' -band images were split up into shorter exposures to ameliorate the effects of sky brightness in the near-infrared. As we were the first science users of ISPI, a better understanding of the instrument, along with changes in the electronics between observing runs, resulted in our group adjusting the exposure time splits for the second observing run. Specifically, due to the range over which the ISPI detector is linear, we discovered the need to split up the J -band images into shorter exposures in order to keep many of the stars from falling into the non-linear regime. In addition, for all three bands, short exposures (4s at each dither point) were needed to avoid saturating the brightest stars in the frame. In Table 1, we detail the exposures times for each band and observing run and in Table 2 we list our target clusters along with their positions on the sky, the filters in which they were observed, and the run during which each cluster was imaged. For all but one of the clusters observed during both runs, only the short (4s) exposures were taken during the second run; the exception to this is NGC 2155, for which the entire set of K' exposures was obtained during the second run.

2.2. Reduction

We have processed our data using standard data reduction techniques. All images have been dark subtracted, sky subtracted and then flat fielded using on-off dome flats. For each target, sky frames were created by median combining the dithered cluster images, thus eliminating the stars and leaving only the sky in the final combined sky frame. Before shifting and combining our cluster images we had to address the problem of geometric distortions. ISPI's large field of view causes images to be curved at the focal plane and, if not corrected, final frames created by shifting and combining the dithered images will have severely degraded image quality across much of the frame. This problem was exacerbated by the large offsets in our dither pattern. Using Galactic bulge star data kindly provided by A. Stephens (2003, private communication), we created and applied a high order distortion correction to our images using the IRAF tasks *geomap* and *geotran*. Corrected images were then aligned, shifted, and average combined and bad pixels were masked to create a final science image for each cluster and filter. The final image quality was excellent and only stars near the corners of the frame exhibited any signs of distortion. We note that for each cluster, we have created two science images in each band; a short exposure image, created by combining only the 4s exposures from each dither point, and a long exposure that is a combination of all data for a given cluster. As mentioned in §2.1, the short exposures were necessary for accurate photometry of the bright RGB stars. In Fig. 1, we present K' -band images of an $\sim 4' \times 4'$

region around each of our target clusters. We have used the final combined long exposure image for each cluster

2.3. Photometry

Using a combination of DAOPHOT and ALLSTAR (Stetson 1987), we have photometered our images with the following method. A rough PSF was created from the brightest ~ 200 stars in each image; we have made sure to only choose stars that were in the linear regime of the detector. This rough PSF was then used to remove neighbors from around the full set of $\sim 50\text{-}150$ PSF stars (depending on cluster), which allowed us to create a more robust PSF from the cleaned image. Next, ALLSTAR was used to fit the improved PSF to all stars that were detected in the science frames. In an effort to detect and photometer faint stars and/or companions, we performed a single iteration where we subtracted all stars photometered in the first ALLSTAR pass, searched for previously undetected stars, and then measured all of the new detections and added them to the photometry list. Aperture corrections, calculated for each science frame, were then applied to the PSF photometry. Lastly, we combined the aperture corrected photometry lists for each filter with the requirement that a star be detected in all available bands for it to be included in the final combined list of instrumental magnitudes.

Finally, to calibrate the instrumental photometry for each cluster, we began by matching stars in common between our long and short exposures, then throwing out stars that are non-linear or saturated (are bright) in the long exposures or have large errors (are faint) in the short exposures. Typically, we are left with intermediate brightness stars covering a range of ~ 2 mag over which we calculate the offset necessary to bring the long exposure photometry onto the ‘system’ of the short exposures. For clusters imaged over two epochs (see Table 2), we find different magnitude offsets between the long and short exposures as compared to clusters observed during only the second observing run. This difference is likely due to different sky conditions during our two observing runs. After offsetting the long exposure photometry, we combine the long and short photometry in three pieces; the bright star photometry is taken from only the short exposures (long exposures are non-linear or saturated) while the faint stars come only from the offset long exposure photometry (stars have large errors or are not detected in the short exposures). The intermediate brightness stars, which have good photometry from both the long and short exposures, are averaged together for the final catalog of each cluster. To put our photometry onto a standard system, we match our stars with those in the All-Sky Data Release of the Two Micron All Sky

Survey¹ (2MASS). We have restricted the 2MASS selection to only those stars possessing either aperture or PSF fitting photometry and having errors less than 0.1 mag. Zeropoint offsets for each band are then calculated and applied to our photometry. In the last step of our calibration, we follow the approach of GS02 and convert our photometry (on the 2MASS system) to the Bessell & Brett (1988) system using the conversions presented by Carpenter (2001, their Eqs. A1-A4). This step is necessary as it places our photometry on the same system as the Girardi & Salaris (2001) models (see §4). We note that we have not fit any color terms in our calibration due to the small range in color (~ 0.5 mag) covered by the RGB in addition to the similarity of the ISPI and 2MASS filter systems.

3. Cluster Ages and Abundances

As mentioned in §1, GS02 showed that knowledge of a populous cluster’s age and metallicity is imperative to accurately predicting M_K^{RC} , and thus determining the cluster’s distance. This is especially true for clusters with $\log(\text{Age}) \lesssim 9.3$ ($\lesssim 2$ Gyr) or $[\text{Fe}/\text{H}] \lesssim -0.4$, two regions of parameter space where M_K^{RC} can vary rapidly (see Figs. 5 and 6 in GS02) and in which many LMC clusters reside.

For the cluster metallicities, we turn primarily to the recent work of Grocholski et al. (2006). In their paper, they present $[\text{Fe}/\text{H}]$ for 28 populous LMC clusters, derived from the strong near infrared absorption lines of the Ca II triplet; all but four of the clusters in our sample (ESO 121-03, NGC 1783, NGC 1978, and SL 896) have metallicities in Grocholski et al. (2006). Red giants in NGC 1783 were studied by A. A. Cole et al. (2007, in preparation) using the Ca II triplet in an almost identical approach to that of Grocholski et al. (2006), so we adopt their metallicity (-0.47 ± 0.14 dex) for this cluster. For NGC 1978, we use the metallicity calculated by Ferraro et al. (2006), which is based on high resolution spectra of 11 red giant stars. We note that their value of -0.38 ± 0.07 dex is in good agreement with the results of A. A. Cole et al. (2007, in preparation), who find $[\text{Fe}/\text{H}] = -0.35 \pm 0.07$. Using UVES on the VLT, Hill et al. (2000) obtained high resolution spectra for two giant stars in ESO 121-03 and found $[\text{Fe}/\text{H}] = -0.91 \pm 0.16$, which we will adopt for this paper. Finally, while the small cluster SL 896 has no previously published spectroscopically derived $[\text{Fe}/\text{H}]$ available, the results of Grocholski et al. (2006) show that the intermediate metallicity LMC clusters have a very tight spread in metallicity ($\sigma = 0.09$), with a mean metallicity of -0.48 dex. Thus, we adopt these values as the metallicity and error for SL 896. Cluster metallicities and errors are presented in columns 2 and 3 of Table 3.

¹<http://www.ipac.caltech.edu/2mass/releases/allsky>

As for the ages, the most reliable way to determine cluster ages is by comparing the predictions of theoretical isochrones to the luminosity of a cluster’s main sequence turn off. However, no large scale database of main sequence fitting (MSF) ages exists for LMC clusters. To address this shortcoming, we have begun to compile optical photometry that reaches below the main sequence turn off (MSTO) for a large number of LMC clusters. While the entire study will be presented in a future paper (Grocholski et al. 2007, in preparation), we herein provide a brief description of the data set and fitting method that are used to derive cluster ages, as well as present ages for a sub-sample of clusters. Optical photometry was taken primarily from the literature and in column 7 of Table 3, we list the CMD sources. In a few cases, we have used unpublished optical images, obtained with either VLT FORS2 (NGC 1846, NGC 2203, IC 2146; see Grocholski et al. 2006) or *HST* WFPC2 (NGC 2193; program number GO-5475). For the three clusters with V and I band VLT FORS2 images, stars were identified and photometered with the aperture photometry routines in DAOPHOT (Stetson 1987) and then matched to form colors. Currently, the photometry for these three clusters is uncalibrated; however, the color terms for the FORS2 array are small (~ 0.03 in $V - I$) and thus have little effect on the shape of the MSTO/RC region, which spans a color range of only ~ 0.6 mag in $V - I$. Regarding NGC 2193, the one cluster in our initial sample with unpublished *HST* WFPC2 photometry, we retrieved F450W and F555W images from the HST archive. These pipeline processed images were photometered via the procedure outlined by Sarajedini (1998), including the Holtzman et al. (1995) transformation coefficients. Since the photometric zero points for WFPC2 are relatively uncertain, and the FORS2 data are uncalibrated, we proceed with MSF as follows. Utilizing the $Z = 0.008$ ($[Fe/H] \approx -0.4$) and $Z = 0.004$ ($[Fe/H] \approx -0.7$) theoretical models from the Padova group (Girardi et al. 2002), which include treatment for core overshoot, we first shift the isochrones vertically to match the brightness of the RC and then move them horizontally to match the color of the unevolved main sequence. For illustrative purposes, NGC 1651 and NGC 2173 are shown in Fig. 2, with the $Z = 0.008$ isochrones over plotted for $\log(\text{Age}) = 9.25$ and 9.30 for NGC 1651 and 9.15 , 9.20 , and 9.25 for NGC 2173; based on these fits, we adopt ages of $\log(\text{Age}) = 9.28$ (1.91 Gyr) and 9.20 (1.58 Gyr) for NGC 1651 and NGC 2173, respectively, and we estimate the error in our fits to be ± 0.05 in terms of $\log(\text{Age})$. Table 3 gives MSF ages for all clusters in our preliminary sample with available optical photometry. While neither NGC 1783 nor NGC 1978 has reliable photometry available in the literature, both have ages determined by Geisler et al. (1997), who used the difference in V -band magnitude between the cluster’s RC and main sequence turnoff to estimate cluster ages. For clusters in common, we find an offset of 0.03 in $\log(\text{Age})$, where our MSF ages are younger than their ages. Therefore, for NGC 1783 and NGC 1978, we offset the values in Geisler et al. (1997) and adopt these as the ages for NGC 1783 and NGC 1978.

4. Apparent and Absolute K -band RC Magnitudes

To calculate the apparent and absolute RC magnitudes, we generally follow the method prescribed by GS02. They determine the apparent K -band magnitude of the RC (K_{RC}) by placing a standard sized box (0.8 mag in K and 0.2 mag in $J - K$) around the RC; the median value of all stars within this box is taken as K_{RC} . A constant box size is used in conjunction with the median magnitude of the RC in an effort to eliminate any selection effects that may occur in choosing the location of the box, as well as to limit the effects of outliers on K_{RC} . In a few cases, we have had to shift the box center slightly in color so as to avoid contamination from RGB stars. For predicting the absolute RC magnitude (M_K^{RC}), GS02 combined available 2MASS photometry (JK_S) for 14 Galactic open clusters, which also have internally consistent ages, abundances, and distances, with an interpolation routine based on low order polynomials. The interpolation over the open clusters allows the prediction of M_K^{RC} for a target cluster with a known age and [Fe/H]. This method was applied to NGC 2158 by GS02 and to Hodge 4 and NGC 1651 by Sarajedini et al. (2002), all with promising results.

Given ISPI’s large field of view, before we can measure K_{RC} we must separate the cluster stars from the field by performing radial cuts on our data. Where available, we use the cluster radii as determined by Grocholski (2006), which were based on the kinematics of individual stars; typically, the farthest star from the cluster center that is moving at the velocity of the cluster denotes the adopted radius. For the four clusters not in common with their study, radial cuts were chosen by eye, using a combination of cluster images and our photometric catalogs. We note that small variations in the adopted cluster radii have no appreciable effect on our results; a change in radius of ± 100 pixels (~ 0.5 arcmin) results in a change in M_K^{RC} of ~ 0.03 mag. In Fig. 3, we present the resulting K vs. $J - K$ cluster CMDs, which extend from the tip of the RGB to ~ 1.5 mag below the helium burning RC; the standard size box used in calculating K_{RC} is shown. For each cluster, the measured value of K_{RC} is given in column 2 of Table 4, along with the standard error of the median (column 3) and number of RC stars in each box (column 4).

Ideally, we would like to predict M_K^{RC} using the open cluster data presented in GS02. In practice, however, this is difficult since our LMC cluster sample falls outside of the parameter space (in metallicity) covered by the open clusters; tests of an extrapolation routine applied to the target cluster abundances proved to be unreliable. Instead, we turn to the theoretical models of Girardi & Salaris (2001, see also Girardi et al. 2000), which provide expected values of M_K^{RC} that span a large range of ages and metallicities and encompass our LMC target clusters. GS02 tested their open cluster data against these theoretical models and found good agreement, with all clusters lying within 1.5σ of the appropriate model and no

systematic offset. Since their comparison was based on data from the Second Incremental Data Release of the 2MASS Point Source Catalog, we have recompared the models and the data, using the updated 2MASS All Sky Data Release. With the new 2MASS photometry, we still find good agreement with the models, however, there is now an offset of 0.08 mag, in that the observed RC values are brighter than what is predicted by the models. We discuss this in more detail in §5.4. Given the ages and metallicities listed in Table 3, we are able to determine M_K^{RC} for each LMC cluster by interpolating over the Girardi & Salaris (2001) models; predicted values of M_K^{RC} are presented in Table 4. The quoted error in M_K^{RC} is calculated by adding in quadrature the effects of age and abundance errors on the predicted absolute RC magnitude. We note that the five youngest clusters in our sample have relatively large error bars due to the fact that their ages place them in a region where the RC brightens rapidly with increasing age (see Fig. 4 in GS02); thus, small errors in age result in large errors in M_K^{RC} .

5. Cluster Distances and the Distance to the LMC

5.1. Absolute Distance Moduli

With K_{RC} and M_K^{RC} in hand, cluster reddening are all that is needed to calculate absolute distance moduli. The extinction maps of both Burstein & Heiles (1982) and Schlegel, Finkbeiner, & Davis (1998) cover the entire LMC; however, Schlegel et al. (1998) were not able to resolve the temperature structure in the inner portions of the LMC and, therefore, could not estimate the reddening reliably. For most clusters, the two reddening maps give values in good agreement, although as some of our clusters lie in the unresolved region, we adopt $E(B-V)$ values solely from Burstein & Heiles (1982) and assume an error of 20%. Reddenings are converted to A_K using the extinction law of Cardelli, Clayton, & Mathis (1989), where $R_V = 3.1$ and $A_K = 0.11A_V$. We note that, since A_K is approximately one third of $E(B-V)$, any differences between the two extinction maps are ultimately negligible. We also note that the adopted values of A_K are typically on the order of the error in measuring K_{RC} . In Table 4 we give $E(B-V)$ and A_K for the cluster sample. With absolute and apparent RC magnitudes and reddening for each cluster, absolute distance moduli, $(m - M)_0$, are readily calculated and are listed in Table 4 along with the distance errors, which are found by adding in quadrature the errors in K_{RC} , M_K^{RC} , and $E(B-V)$.

5.2. LMC Cluster Distribution

It has long been known that the disk of the LMC is inclined with respect to the plane of the sky (see e.g., Caldwell & Coulson 1986), and this inclination is an important effect when using individual stars (or clusters) to determine the distance to the LMC center. Recent work using field stars as a tracer of the disk (tip of the RGB and AGB, van der Marel & Cioni 2001; field RC stars, Olsen & Salyk 2002; carbon stars, van der Marel et al. 2002; Cepheid variables, Nikolaev et al. 2004) has shown that the LMC has an inclination of $i \sim 31^\circ - 36^\circ$, with a position angle of the line of nodes, Θ , between 120° and 150° ; both of these quantities have the standard definitions where $i = 0^\circ$ for a face on disk and Θ is measured counterclockwise from north. The LMC centers adopted by each of these authors, in addition to their derived values for Θ and i , are given in Table 5. In Fig. 4 we plot the positions on the sky of our target clusters as well as the LMC centers adopted by van der Marel & Cioni (2001, *filled square*), van der Marel et al. (2002, *filled triangle*), and Olsen & Salyk (2002, *filled star*). The solid lines passing through these points show each author’s position angle of the line of nodes. We note that, for clarity, we have not plotted the center and position angle of the line of nodes from Nikolaev et al. (2004) as they are very similar to the values in Olsen & Salyk (2002). For reference, the 2° near-infrared isopleth (van der Marel 2001), which roughly outlines the LMC bar, is plotted as the dashed ellipse. Conversion to Cartesian coordinates from right ascension and declination was performed using a zenithal equidistant projection (e.g., van der Marel & Cioni 2001, their eqs. [1]-[4]); lines of right ascension and declination have been marked with dotted lines. In general, these geometries tell us that the northeast portion of the LMC is closer to us than the southwest. More specifically, since points along the line of nodes are equidistant from the observer, in the direction perpendicular to the line of nodes we would expect to see a maximum gradient in cluster distance.

To compare our cluster distribution with the geometry of the LMC, in Fig. 5 we plot cluster distance as a function of radial distance along the line of maximum gradient. While we have used the geometry of van der Marel & Cioni (2001) to determine the position of the line of maximum gradient, the choice in LMC geometry between these three recent studies has little effect on the results (see §5.3). In the top panel, clusters are labeled for reference and in the bottom panel we have included the 1σ distance errors. In addition, the dashed line represents the disk of the LMC, where the LMC center ($x = 0$) has a distance of 47.9 kpc (see §5.3) and $i = 34.7^\circ$ (van der Marel & Cioni 2001); the dotted line represents a constant disk thickness of ± 1 kpc. While a flared disk model (Alves & Nelson 2000) is probably a more correct representation of the LMC’s disk, for the purposes of our comparison a constant thickness disk model is adequate. Regardless, Fig. 5 shows that, with the exception of the youngest clusters, which have inherently uncertain distances, our results are consistent with the idea that the LMC clusters lie in the same inclined, thick disk as defined by a variety of

field populations.

A disk-like cluster distribution is as expected, based on the kinematics of the cluster system (Schommer et al. 1992), but this is the first time it has been demonstrated that the clusters and field stars reside in the same disk. This result is in contrast to the recent findings of Kerber et al. (2006), who used the MSTO to calculate distances for 15 LMC clusters. From their data they found a disk-like distribution for their clusters, along with an inclination of $39^\circ \pm 7^\circ$, which is $\sim 8^\circ$ steeper than the $30.7^\circ \pm 1.1^\circ$ disk inclination that Kerber et al. (2006) adopted from Nikolaev et al. (2004). Kerber et al. (2006) interpreted this inclination difference as suggesting that the LMC’s intermediate-age clusters formed in a different disk than the field stars. However, they discuss neither the results of van der Marel & Cioni (2001) nor Olsen & Salyk (2002), who find disk inclinations of $34.7^\circ \pm 6.2^\circ$ and $35.8^\circ \pm 2.4^\circ$, respectively, both in agreement with the cluster disk inclination found by Kerber et al. (2006).

We note in passing that Olsen & Salyk (2002) found what appears to be a warp in the southwest portion of the LMC. Their fields in this region are brighter than expected, giving the impression that they have been pulled toward the MW. There is, however, a possible problem with the reddening corrections that Olsen & Salyk (2002) have applied to these fields, which may explain the apparent warp. As only two of our target clusters, NGC 1651 and SL 61, lie in the warped area, we are not in a position to comment on their result.

Since galactic disks are relatively fragile, and it is highly unlikely that clusters would form in a halo and then be perturbed into a disk, the disk-like distribution and kinematics of our LMC clusters suggest that they formed in a disk. As ESO 121 is the oldest cluster in our IR sample, its residence in the LMC’s disk implies that the disk formed ~ 9 Gyr ago. However, ESO 121 is well known to be the only cluster in the LMC with an age between approximately 3 Gyr and 13 Gyr. To further explore the age of the disk, we turn to the LMC’s *bona fide* old (~ 13 Gyr) globular cluster population and the optical photometry of A. R. Walker (see Walker 1985; Walker & Mack 1988; Walker 1989, 1990, 1992a,b, 1993). Walker measured the mean apparent V -band magnitude (V_{RR}) of RR Lyrae stars in seven LMC globular clusters and, using their pulsational properties, was able to estimate cluster metallicities. Given the metallicity of a cluster, the mean absolute RR Lyrae magnitude is determined by $M_V^{RR} = 0.23[Fe/H] + c$ (Chaboyer 1999), and by adopting reddenings from Burstein & Heiles (1982) we can readily calculate distances for these seven clusters. The zeropoint, c , in the above relation is chosen such that NGC 1835 lies on the dashed line. Cluster information is given in Table 7, and these new data points are plotted in Fig. 5 as open circles, along with their 1σ errors. The errors in [Fe/H] and V_{RR} are taken from Walker and we assume a 20% error in $E(B-V)$ for all clusters except Reticulum, for which we adopt 0.02 mag. Fig. 5 shows that, like the intermediate age clusters, the old globular

clusters are distributed in a manner that is consistent with the thick, inclined disk geometry of the LMC field stars. The agreement between the old globular clusters and the disk suggest that cluster like NGC 2257 and NGC 1466 formed in, and still reside in, the disk. The disk of the LMC, therefore, must be roughly the same age as the globular clusters, ~ 13 Gyr old.

Lastly, we note the position of NGC 1841. This cluster resides ~ 12 kpc from the LMC center (to the south), which places it near the tidal radius ($r_t = 15.0 \pm 4.5$ kpc, van der Marel et al. 2002) of the LMC, and, as can be seen in Fig. 5, it sits well out of the plane of the disk, in the direction of the Milky Way. Thus, NGC 1841 is likely to have either been pulled out of the disk, or stripped from the LMC altogether, in a close encounter with the Milky Way.

5.3. The Distance to the LMC Center

For any given point, P , that resides in the disk of the LMC, the distance, D , of that point is related to the distance to the center of the LMC, D_0 , by

$$D/D_0 = \cos i / [\cos i \cos \rho - \sin i \sin \rho \sin(\phi - \theta)], \quad (1)$$

where i is the inclination of the disk and $\theta = \Theta + 90^\circ$ (see van der Marel & Cioni 2001 for a detailed discussion of equations 1–4). The angular coordinate ρ is defined as the angular separation on the sky between P and the LMC center, while ϕ is the position angle of P relative to the center. Typically, ϕ is measured counterclockwise from the axis that runs in the direction of decreasing right ascension and passes through the LMC center. These coordinates (ρ, ϕ) can be uniquely defined by the cosine and sine rule of spherical trigonometry and the analog formula, which give

$$\cos \rho = \cos \delta \cos \delta_0 \cos(\alpha - \alpha_0) + \sin \delta \sin \delta_0, \quad (2)$$

$$\sin \rho \cos \phi = -\cos \delta \sin(\alpha - \alpha_0), \quad (3)$$

and

$$\sin \rho \sin \phi = \sin \delta \cos \delta_0 - \cos \delta \sin \delta_0 \cos(\alpha - \alpha_0). \quad (4)$$

In equations 2–4, α_0 and δ_0 are the right ascension and declination of the LMC center while α and δ mark the position on the sky of P . Therefore, since it is reasonable to assume that our target clusters lie in the disk of the LMC, as defined by the field stars (§5.2), we can use the distances of our clusters in conjunction with the LMC geometry to calculate the distance to the center of the LMC.

As an example, we adopt $i = 34^\circ 7$ and $\Theta = 122^\circ 5$ (van der Marel & Cioni 2001), and calculate values for the LMC center distance based on the distance and position of each of our 17 target clusters. Raw cluster distances from Table 4 and the corresponding LMC distance are given in Table 6 with the LMC distance errors calculated by propagating the errors in i , Θ , and D through equation 1. Finally, we calculate the distance to the LMC as the mean of the individual center distances, for which we find $D_0 = 47.9 \pm 0.9$ kpc, or $(m - M)_0 = 18.40 \pm 0.04$; the quoted error is the standard error of the mean. We note that, while calculating the straight mean does include the young clusters, which have uncertain distances, we have found that the mean, median, weighted mean, and 2σ clipped mean all give distances within 0.01 mag of each other, thus we have chosen to simply adopt the mean as our final distance. In addition to van der Marel & Cioni (2001), we also use the geometry of Olsen & Salyk (2002), van der Marel et al. (2002), and Nikolaev et al. (2004) to calculate the distance to the LMC, with all four mean distances given in Table 5. The final distances, $D_0 = 47.9 \pm 0.9$ kpc, 48.1 ± 0.9 kpc, 47.9 ± 0.9 kpc, and 48.1 ± 0.9 kpc, are all in excellent agreement, which shows that the choice of geometry between these four authors has little effect on the distance to the LMC center.

5.4. Systematic Errors

An analysis of our approach to calculating cluster distances gives two possible sources of systematic errors. The first source of error in our calculations arises from our interpolation method. As discussed in §4, due to the location of our target clusters in the age-metallicity parameter space, we are not able to interpolate over the open cluster data in GS02. Instead, we have had to use the theoretical models of Girardi & Salaris (2001) for our interpolation. While the models are in good agreement with the open cluster data, they predict absolute magnitudes that are, on average, 0.08 mag fainter than what is observed. An additional systematic error may arise from our choice of reddening map. Burstein & Heiles (1982) zeropoint their reddening maps to an area near the north galactic pole which was long believed to be a direction of zero reddening. Schlegel et al. (1998), however, find $E(B-V) = 0.02$ mag for the same location on the sky. These two systematic errors work in opposite directions; if we applied a correction for the interpolation error, clusters would move *closer*, while a correction for the reddening error would make them appear farther away. However, since $A_K = 0.341E(B-V)$, the systematic reddening error is small and is dominated by the systematic error due to our interpolation. Therefore, we adopt 0.08 mag as our systematic error.

6. Comparison to Previous Distances

Since an extensive review of LMC distances determined by a variety of standard candles can be found in Clementini et al. (2003), herein we restrict our comparison to only a couple recent distance calculations. The only previous LMC cluster distances based on the K -band luminosity of the RC are presented in Sarajedini et al. (2002) and, using the approach described in GS02, they find $(m - M)_0 = 18.55 \pm 0.12$ and 18.52 ± 0.17 for NGC 1651 and Hodge 4, respectively. Both distances are farther than what we find for the same clusters, due primarily to their photometric calibration. For both clusters, Sarajedini et al. (2002) measure K_{RC} to be ~ 0.1 mag fainter than our values. Given the small number of standard stars used by Sarajedini et al. (2002) along with their small field of view, which provided only a handful of stars for aperture correction determination, this difference in photometric zeropoint is not unexpected.

Most recently, Macri et al. (2006) observed Cepheid variables in two fields in the maser-host galaxy NGC 4258. By comparing the LMC’s Cepheid P-L relation to their observations of variables in NGC 4258, Macri et al. (2006) were able to calculate a *relative* distance between these two galaxies of $\Delta(m - M)_0 = 10.88 \pm 0.04$ (random) ± 0.05 (systematic). Being a maser-host galaxy, NGC 4258 has an accurate geometric distance ($29.29 \pm 0.09 \pm 0.12$ mag) that, combined with the Cepheid-based relative distance, allowed Macri et al. (2006) to calculate the distance to the LMC. They find $(m - M)_0 = 18.41 \pm 0.10 \pm 0.13$, in excellent agreement with our results. As discussed by Marci et al. (2006), this improved distance has implications for calculations of H_0 . The *HST* Key Project to determine the Hubble constant (see Freedman et al. 2001) adopted $(m - M)_0 = 18.5 \pm 0.1$ as their distance to the LMC, which acts as the zeropoint for the extragalactic distance scale. Using this longer distance, Freedman et al. (2001) find $H_0 = 72 \pm 8$ km s $^{-1}$ Mpc $^{-1}$. In recalculating H_0 , Macri et al. (2006) find that the shorter LMC distance increases the Hubble constant $\sim 3\%$. However, they find that their new coefficient of metallicity dependence for Cepheid variables has the opposite effect, changing H_0 by $\sim -2\%$. Thus, the cumulative effect results in only a small change in the Hubble constant. With their new results, they calculate $H_0 = 74 \pm 3 \pm 6$ km s $^{-1}$ Mpc $^{-1}$.

7. Summary

In this paper we have presented results of a near-infrared photometric study of populous clusters in the LMC. Using ISPI on the CTIO 4m we obtained JK' photometry down to ~ 1.5 mag below the core helium burning red clump stars in 17 clusters, allowing us to accurately measure the *apparent* K -band magnitude of the RC. In a similar approach to that of GS02,

we combine cluster ages and metallicities with theoretical models to predict the *absolute K*-band RC magnitude for each of these clusters. Thus, we are able to determine accurate cluster distances and explore the 3-dimensional cluster distribution as well as calculate the distance to the center of the LMC. The main results of our paper are as follows:

- 1) We have compiled deep optical photometry (below the MSTO) for 15 of our clusters. By combining these data with previously published metallicities, we are able to break the well known age-metallicity degeneracy and calculate accurate cluster ages via MSTO fitting with theoretical isochrones that include treatment for core overshoot. The intermediate age clusters range in age from only \sim 1-3 Gyr; thus, these MSF ages do not close the LMC’s cluster age gap. We confirm that ESO 121, the only LMC cluster known to have an age between \sim 3-13 Gyr, formed approximately 9 Gyr ago.
- 2) By combining K_{RC} measured from our near IR photometry with the values of M_K^{RC} predicted by theoretical models, we have determined accurate distances for all 17 clusters in our sample; our average standard error of the mean distance is 0.08 mag, or 1.8 kpc. This work represents the largest sample of LMC clusters with distances derived in an internally consistent way.
- 3) The cluster distances allow us to explore the spatial distribution of the LMC cluster system. Previous work has shown that the LMC field populations lie in a thick, inclined disk and our results illustrate that the clusters are distributed in the same manner. A disk-like distribution for all LMC clusters has been inferred from the kinematics of the cluster system, however, our results mark the first time that it has been demonstrated that the clusters and the field stars lie in the same plane.
- 4) Previously published RR Lyrae data for seven old globular clusters have allowed us to calculate distances for these clusters and compare their distribution to the geometry of the LMC. Like the intermediate age clusters, the globular clusters have a distribution that is consistent with residence in the disk of the LMC.
- 5) Given that it is unlikely for clusters to form in a halo and then be perturbed *into* a disk, the disk-like kinematics and distribution of the LMC clusters implies that they formed in a disk. The fact that old clusters (e.g., NGC 2257, NGC 1466, ESO 121) are seen to currently reside in the disk suggests that they also formed in the LMC’s disk. From this, we infer that the disk of the LMC must have formed about \sim 13 Gyr ago.
- 6) The old globular cluster NGC 1841 lies near the LMC’s tidal radius and well out of the plane of the disk, in the direction of the Milky Way. Its position suggests that it was pulled out of the disk, or possibly stripped from the LMC, in a close encounter with the Milky Way.

7) Taking the inclined geometry of the LMC into account, we find the mean distance to the center of this nearby galaxy to be $(m - M)_0 = 18.40 \pm 0.04 \pm 0.08$ or $D_0 = 47.9 \pm 0.9 \pm 1.8$ kpc. Our result is in excellent agreement with the recent work of Macri et al. (2006) who found $(m - M)_0 = 18.41 \pm 0.1 \pm 0.13$ by comparing Cepheid variables in the maser-host galaxy NGC 4258 with those in the LMC. This distance, however, is ~ 0.1 mag shorter than the commonly accepted distance of 18.5 ± 0.1 mag, which was used in the *HST* Key Project to calculate H_0 (see Freedman et al. 2001). This shorter distance has the effect of increasing H_0 by $\sim 3\%$ (Macri et al. 2006).

This research was supported by NSF CAREER grant AST-0094048 to AS. We would like to thank Mike Barker for assistance with the near-IR observations, Andy Stephens for providing us with a copy of his data, and Steve Eikenberry for helpful discussions regarding the data processing. The authors appreciate the helpful comments of an anonymous referee.

REFERENCES

- Abraham, R. G. 1999, in IAU Symp. 186: Galaxy Interactions at Low and High Redshift, ed. J. E. Barnes & D. B. Sanders, 11–
- Alves, D. R. & Nelson, C. A. 2000, ApJ, 542, 789
- Bessell, M. S. & Brett, J. M. 1988, PASP, 100, 1134
- Bica, E., Geisler, D., Dottori, H., Clariá, J. J., Piatti, A. E., & Santos, Jr., J. F. C. 1998, AJ, 116, 723
- Brocato, E., Di Carlo, E., & Menna, G. 2001, A&A, 374, 523
- Burstein, D. & Heiles, C. 1982, AJ, 87, 1165
- Caldwell, J. A. R. & Coulson, I. M. 1986, MNRAS, 218, 223
- Cardelli, J. A., Clayton, G. C., & Mathis, J. S. 1989, ApJ, 345, 245
- Carpenter, J. M. 2001, AJ, 121, 2851
- Chaboyer, B. 1999, in ASSL Vol. 237: Post-Hipparcos cosmic candles, ed. A. Heck & F. Caputo, 111–+
- Cioni, M.-R. L., van der Marel, R. P., Loup, C., & Habing, H. J. 2000, A&A, 359, 601

- Clementini, G., Gratton, R., Bragaglia, A., Carretta, E., Di Fabrizio, L., & Maio, M. 2003, AJ, 125, 1309
- Ferraro, F. R., Mucciarelli, A., Carretta, E., & Origlia, L. 2006, ApJ, 645, L33
- Freedman, W. L., Madore, B. F., Gibson, B. K., Ferrarese, L., Kelson, D. D., Sakai, S., Mould, J. R., Kennicutt, R. C., Ford, H. C., Graham, J. A., Huchra, J. P., Hughes, S. M. G., Illingworth, G. D., Macri, L. M., & Stetson, P. B. 2001, ApJ, 553, 47
- Geisler, D., Bica, E., Dottori, H., Claria, J. J., Piatti, A. E., & Santos, J. F. C. 1997, AJ, 114, 1920
- Gieren, W. P., Fouque, P., & Gomez, M. 1998, ApJ, 496, 17
- Girardi, L., Bertelli, G., Bressan, A., Chiosi, C., Groenewegen, M. A. T., Marigo, P., Salasnich, B., & Weiss, A. 2002, A&A, 391, 195
- Girardi, L., Bressan, A., Bertelli, G., & Chiosi, C. 2000, A&AS, 141, 371
- Girardi, L. & Salaris, M. 2001, MNRAS, 323, 109
- Grocholski, A. J. 2006, Ph.D. Thesis
- Grocholski, A. J., Cole, A. A., Sarajedini, A., Geisler, D., & Smith, V. V. 2006, AJ, 132, 1630
- Grocholski, A. J. & Sarajedini, A. 2002, AJ, 123, 1603
- Hill, V., François, P., Spite, M., Primas, F., & Spite, F. 2000, A&A, 364, L19
- Holtzman, J. A., Burrows, C. J., Casertano, S., Hester, J. J., Trauger, J. T., Watson, A. M., & Worthey, G. 1995, PASP, 107, 1065
- Kerber, L. O., Santiago, B. X., & Brocato, E. 2006, ArXiv Astrophysics e-prints
- Macri, L. M., Stanek, K. Z., Bersier, D., Greenhill, L., & Reid, M. 2006, ArXiv Astrophysics e-prints
- Madore, B. F. & Freedman, W. L. 1991, PASP, 103, 933
- Mateo, M. & Hodge, P. 1985, PASP, 97, 753
- Nikolaev, S., Drake, A. J., Keller, S. C., Cook, K. H., Dalal, N., Griest, K., Welch, D. L., & Kanbur, S. M. 2004, ApJ, 601, 260

- Olsen, K. A. G. & Salyk, C. 2002, AJ, 124, 2045
- Piatti, A. E., Sarajedini, A., Geisler, D., Bica, E., & Clariá, J. J. 2002, MNRAS, 329, 556
- Sarajedini, A. 1998, AJ, 116, 738
- Sarajedini, A., Grocholski, A. J., Levine, J., & Lada, E. 2002, AJ, 124, 2625
- Schlegel, D. J., Finkbeiner, D. P., & Davis, M. 1998, ApJ, 500, 525
- Schommer, R. A., Suntzeff, N. B., Olszewski, E. W., & Harris, H. C. 1992, AJ, 103, 447
- Schweizer, F. 1999, in IAU Symp. 186: Galaxy Interactions at Low and High Redshift, ed. J. E. Barnes & D. B. Sanders, 1–+
- Stetson, P. B. 1987, PASP, 99, 191
- Udalski, A. 2000, ApJ, 531, L25
- van der Marel, R. P. 2001, AJ, 122, 1827
- van der Marel, R. P., Alves, D. R., Hardy, E., & Suntzeff, N. B. 2002, AJ, 124, 2639
- van der Marel, R. P. & Cioni, M.-R. L. 2001, AJ, 122, 1807
- Walker, A. R. 1985, MNRAS, 212, 343
- . 1989, AJ, 98, 2086
- . 1990, AJ, 100, 1532
- . 1992a, AJ, 103, 1166
- . 1992b, AJ, 104, 1395
- . 1993, AJ, 105, 527
- Walker, A. R. & Mack, P. 1988, AJ, 96, 1362

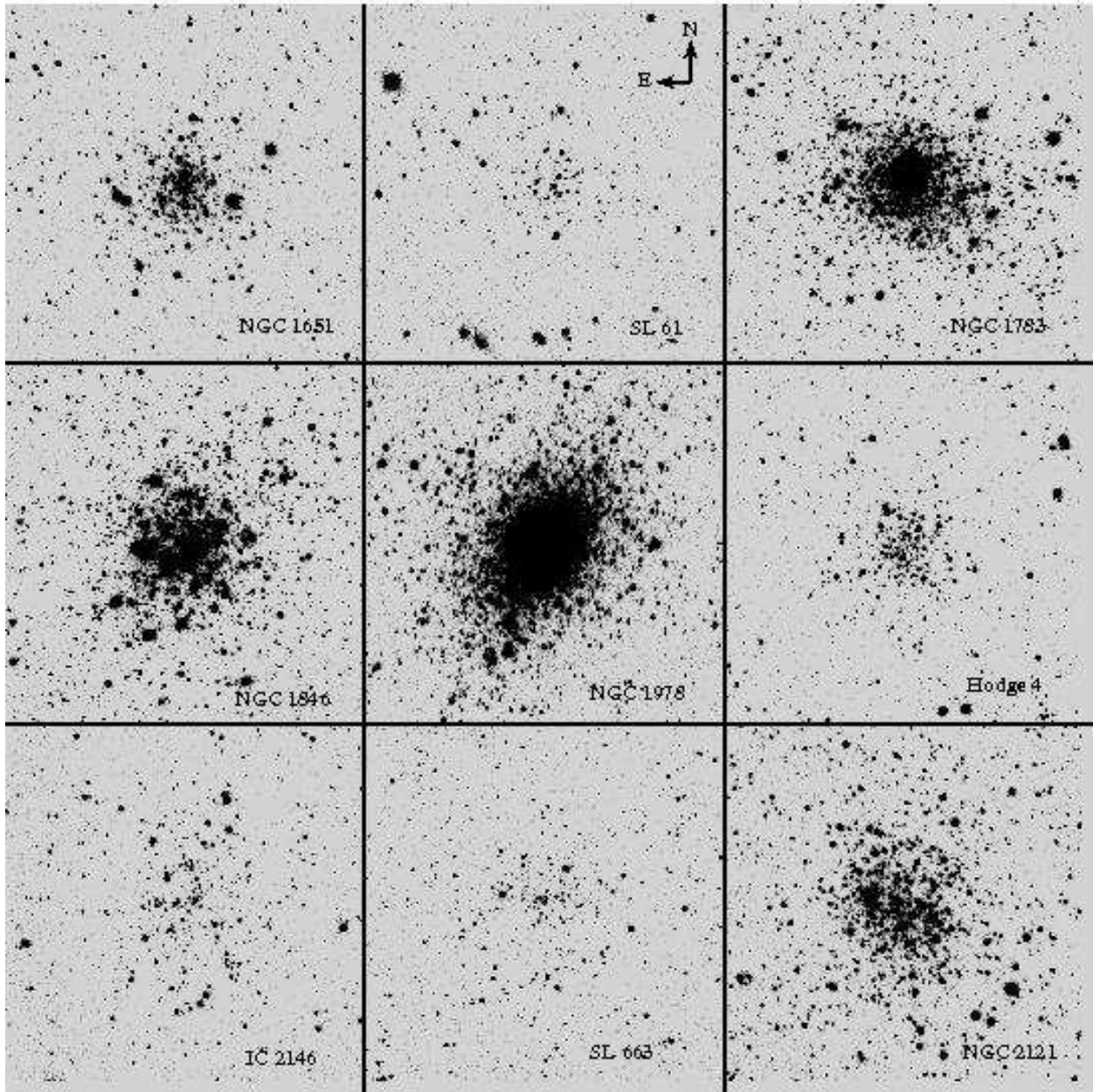


Fig. 1.— K' -band images for all target clusters. We have used the final combined long exposures and selected a region $\sim 4' \times 4'$ in size around each cluster. In all frames, clusters are labeled and the orientation is such that north is up and east is to the left.

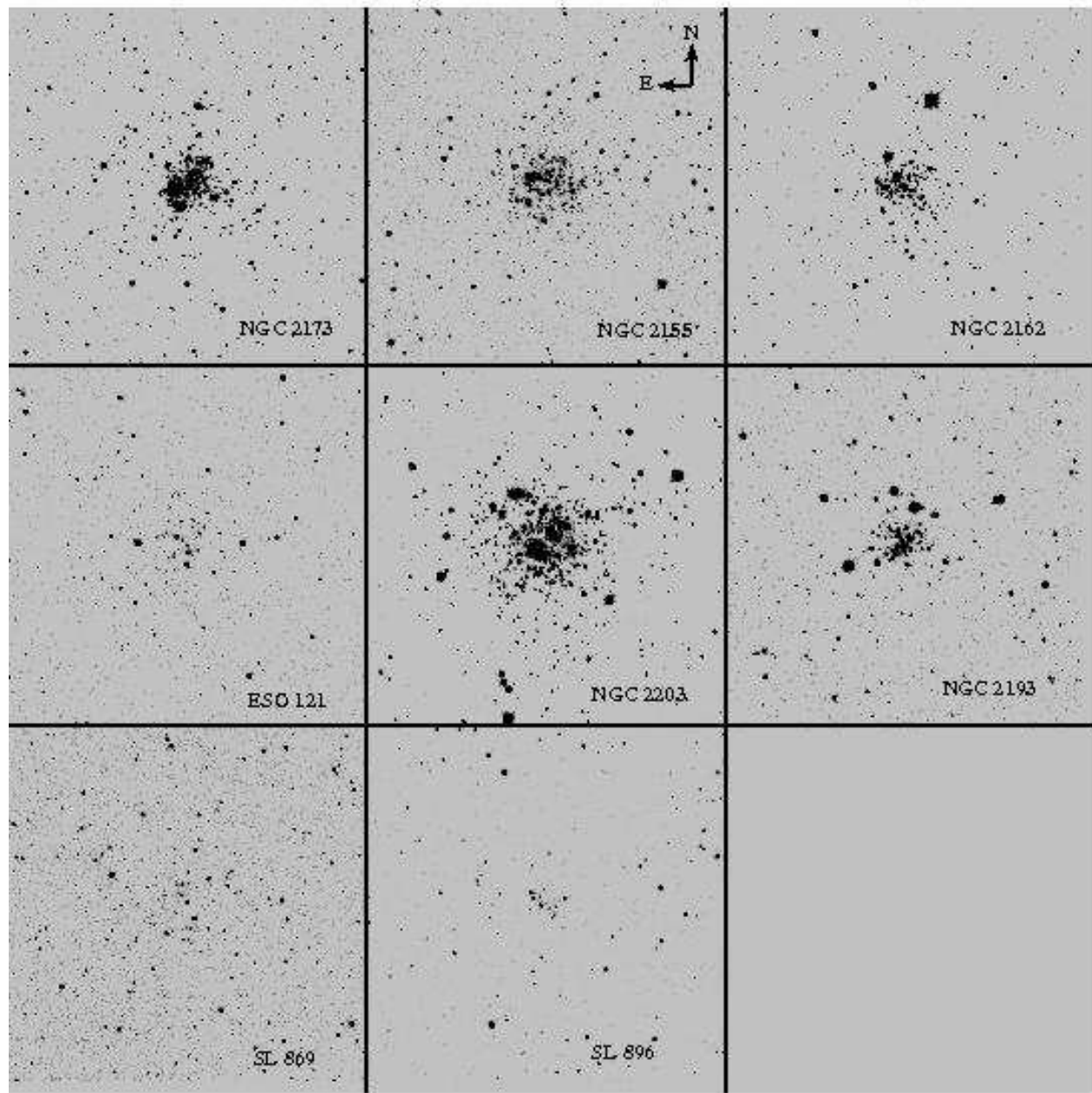


Fig. 1.— - Continued.

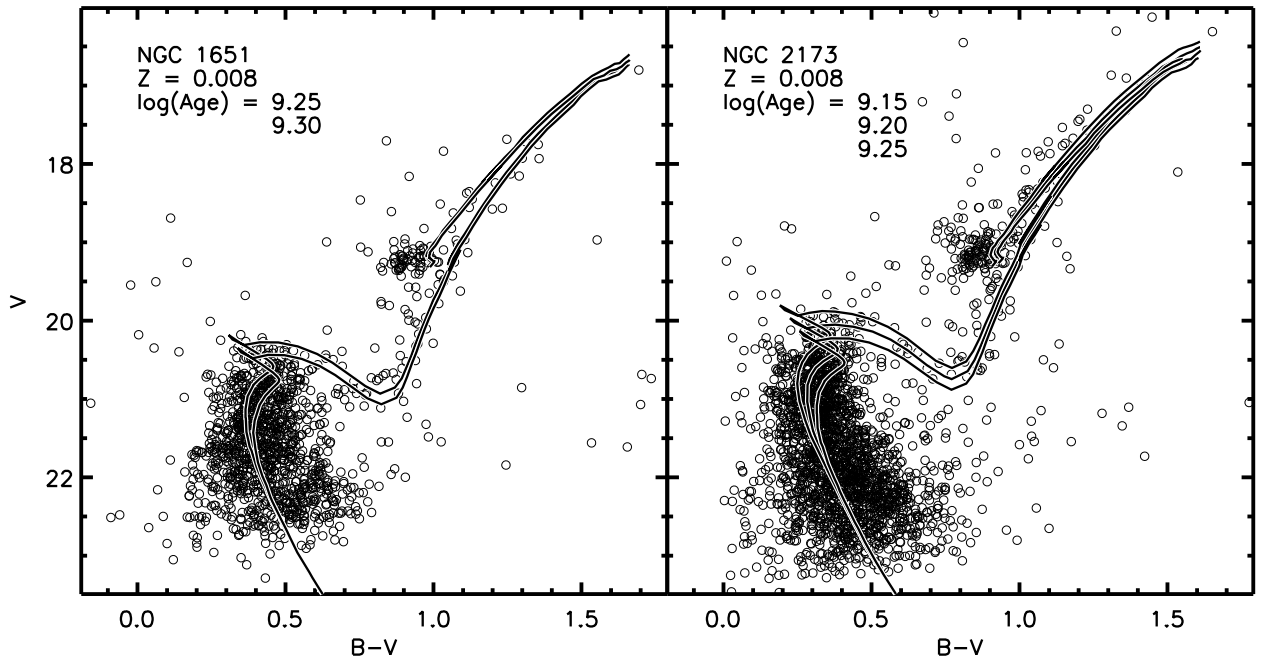


Fig. 2.— Optical photometry for NGC 1651 (left) and NGC 2173 (right), overplotted with the $Z = 0.008$ theoretical isochrones from Girardi et al. (2002); isochrone ages are listed in the figure. These plots illustrate our MSF method where we match isochrones to the brightness of the RC and color of the unevolved main sequence to determine cluster ages.

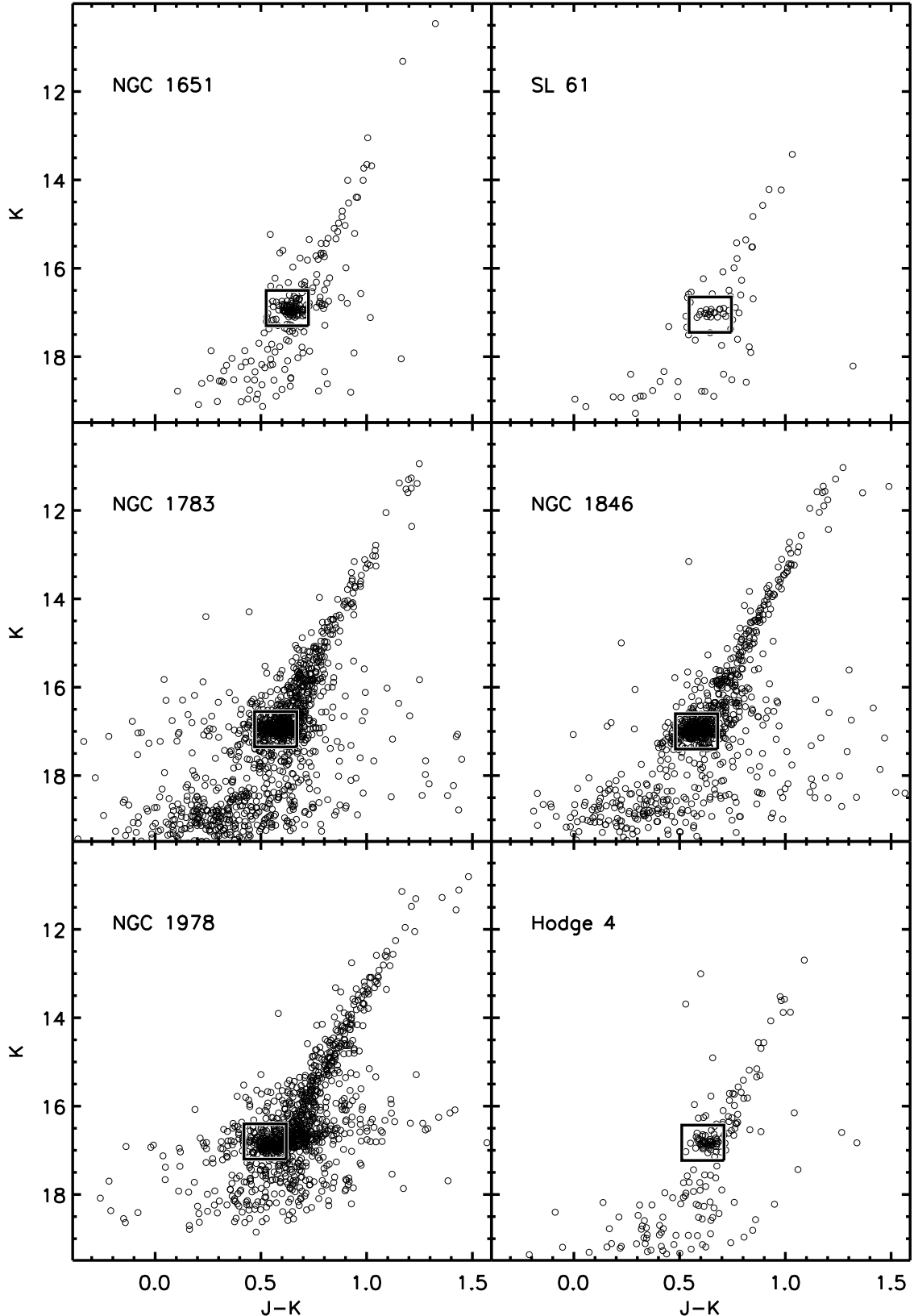


Fig. 3.— Near-infrared CMDs for the 17 clusters in our sample. Cluster RCs are denoted by the box and all stars within this box are used in calculating M_K^{RC} .

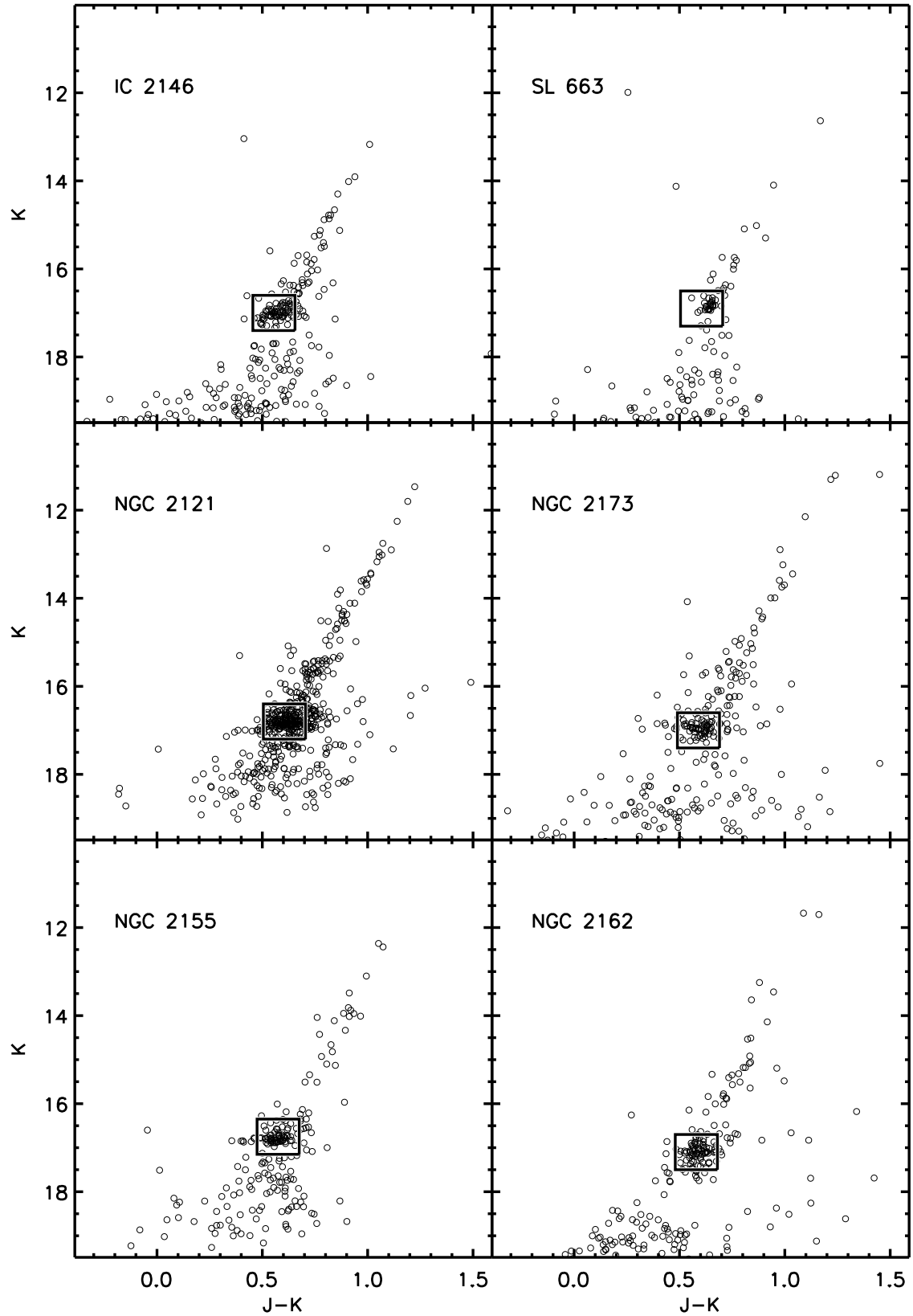


Fig. 3.— *Continued.*

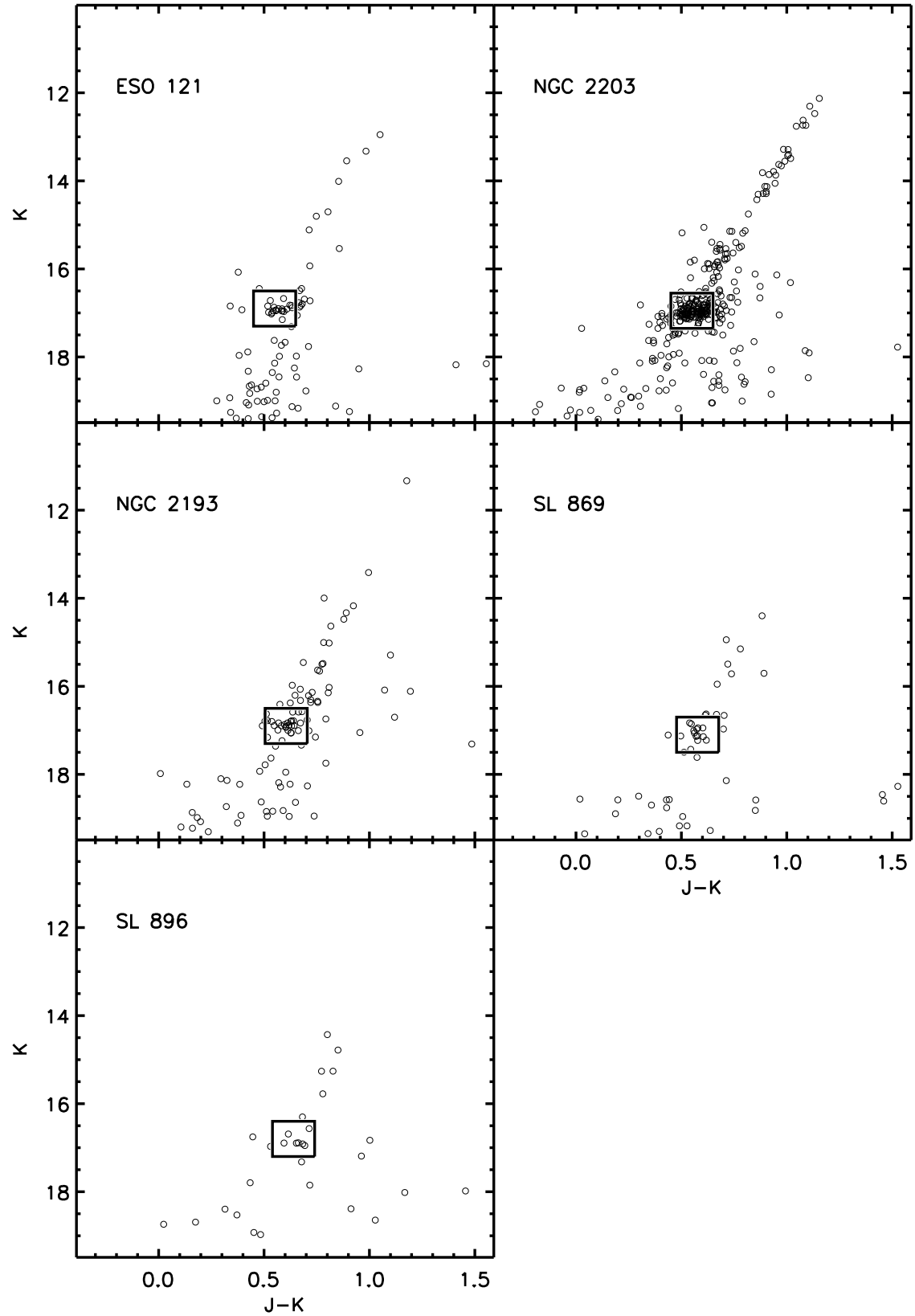


Fig. 3.— *Continued.*

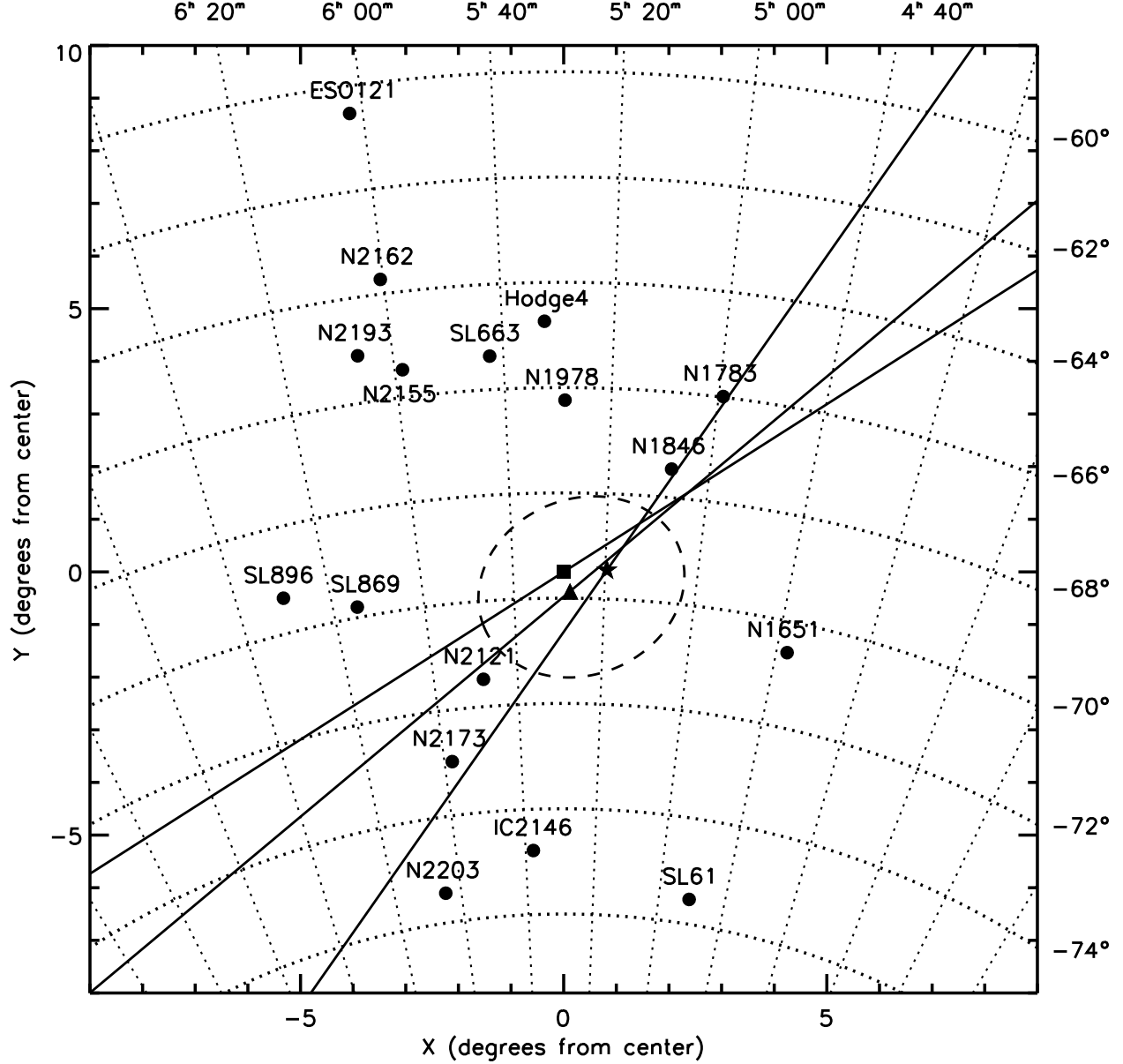


Fig. 4.— Schematic diagram showing the positions on the sky of our target clusters. The dashed ellipse represents the 2° near-infrared isopleth from van der Marel (2001), which roughly outlines the LMC's bar. Also shown are the LMC centers used by van der Marel & Cioni (2001, *filled square*), van der Marel et al. (2002, *filled triangle*), and Olsen & Salyk (2002, *filled star*). The position angle of the line of nodes derived by each of these authors is plotted as the solid line passing through the appropriate LMC center.

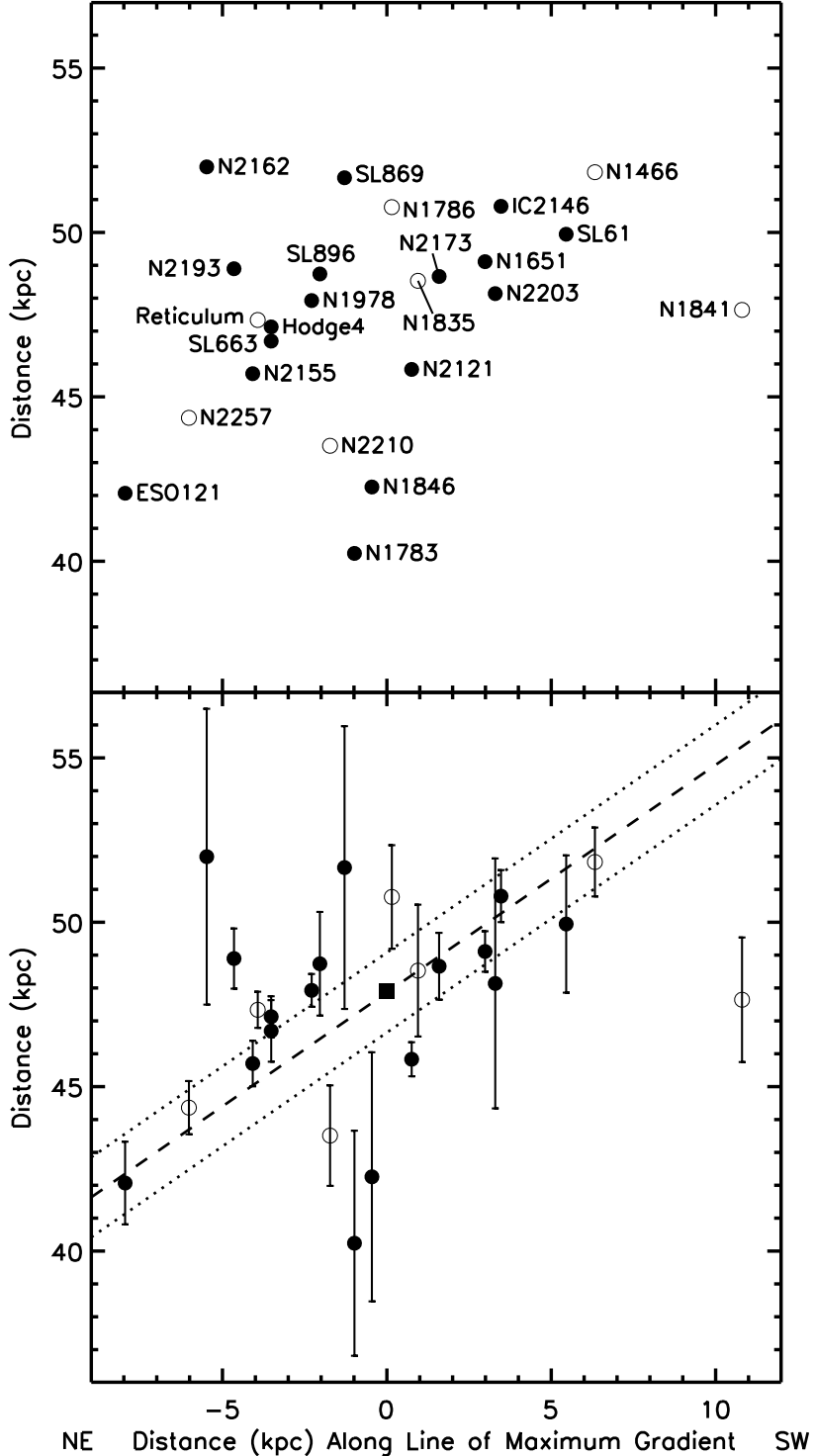


Fig. 5.— Cluster distances as a function of their position along the line of maximum gradient (see §5.2). Open circles mark the old globular clusters from Walker while the filled circles represent the populous clusters in our study. In the bottom panel, the dashed line marks the LMC’s disk with $i = 34.7^\circ$ and $D_0 = 47.9$ kpc (at $x = 0$), and the dotted lines represent a disk thickness of ± 1 kpc; the filled square denotes the center of the LMC. This plot illustrates that both the old and intermediate age clusters are distributed along the disk of the LMC.

Table 1. Exposure Times at Each Dither Point

Dates	J	H	K'
20-22 Jan 2003	60s	15s × 6	10s × 9
06-08 Feb 2004	4s, 20s, 36s	4s, 15s × 6	4s, 10s × 9

Table 2. LMC Cluster Sample Information

Cluster	Alternate Name	R.A. (J2000.0)	Decl. (J2000.0)	Filters	Run
NGC 1651	SL 7, LW 12	4 37 33	−70 35 08	<i>JHK'</i>	1,2
SL 61	LW 79	4 50 45	−75 32 00	<i>J...K'</i>	2
NGC 1783	SL 148	4 59 09	−65 59 14	<i>J...K'</i>	2
NGC 1846	SL 243	5 07 35	−67 27 31	<i>J...K'</i>	2
NGC 1978	SL 501	5 28 45	−66 14 09	<i>JHK'</i>	1,2
Hodge 4	SL 556, LW 237	5 32 25	−64 44 12	<i>JHK'</i>	1,2
IC 2146	SL 632, LW 258	5 37 46	−74 47 00	<i>J...K'</i>	2
SL 663	LW 273	5 42 29	−65 21 48	<i>J...K'</i>	2
NGC 2121	SL 725, LW 303	5 48 12	−71 28 52	<i>JHK'</i>	1,2
NGC 2173	SL 807, LW 348	5 57 58	−72 58 41	<i>J...K'</i>	2
NGC 2155	SL 803, LW 347	5 58 33	−65 28 35	<i>JHK'</i>	1,2
NGC 2162	SL 814, LW 351	6 00 30	−63 43 19	<i>J...K'</i>	2
ESO 121-03		6 02 03	−60 31 26	<i>JHK'</i>	1,2
NGC 2203	SL 836, LW 380	6 04 43	−75 26 18	<i>J...K'</i>	2
NGC 2193	SL 839, LW 387	6 06 18	−65 05 57	<i>JHK'</i>	1,2
SL 869	LW 441	6 14 41	−69 48 07	<i>JHK'</i>	2
SL 896	LW 480	6 29 58	−69 20 00	<i>JHK'</i>	1,2

Note. — Units of right ascension are in hours, minutes, and seconds and units of declination are in degrees, arcminutes, and arcseconds.

Table 3. LMC Cluster Ages and Metallicities

Cluster	[Fe/H] ^a	$\sigma_{[Fe/H]}^a$	Log Age	Age (Gyr)	CMD Ref.
NGC 1783	−0.47 ^b	0.14 ^b	9.08 ^d	1.20	—
NGC 1846	−0.49	0.03	9.10	1.26	7
NGC 2162	−0.46	0.07	9.15	1.41	1
NGC 2203	−0.41	0.03	9.15	1.41	7
SL 869	−0.40	0.04	9.15	1.41	6
SL 61	−0.35	0.04	9.18	1.51	4
NGC 2173	−0.42	0.03	9.20	1.58	1
IC 2146	−0.41	0.02	9.25	1.78	7
NGC 1978	−0.38 ^c	0.07 ^c	9.27 ^d	1.86	—
NGC 1651	−0.53	0.03	9.28	1.91	1
NGC 2193	−0.49	0.05	9.30	2.00	3
Hodge 4	−0.55	0.06	9.33	2.14	5
SL 896	−0.48 ^e	0.09 ^e	9.33	2.14	6
NGC 2155	−0.50	0.05	9.45	2.82	1
SL 663	−0.54	0.05	9.45	2.82	1
NGC 2121	−0.50	0.03	9.48	3.02	5
ESO 121-03	−0.91 ^f	0.16 ^f	9.95	8.91	2

Note. — Optical photometry used to construct the CMDs comes from the following sources: (1) Brocato et al. (2001); (2) Bica et al. (1998); (3) HST GO-5475; (4) Mateo & Hodge (1985); (5) Sarajedini (1998); (6) Piatti et al. (2002); (7) Grocholski et al. (2007, in prep)

^aFrom Grocholski et al. (2006), unless noted.

^bFrom Cole et al. (in prep)

^cFrom Ferraro et al. (2006)

^dAges adjusted from Geisler et al. (1997)

^eMean value of the intermediate metallicity clusters from Grocholski et al. (2006)

^fFrom Hill et al. (2000)

Table 4. Calculated Red Clump Values and Cluster Distances

Cluster Name	K_{RC}	$\sigma_{K_{RC}}$	n Stars	M_K^{RC}	$\sigma_{M_K^{RC}}$	$E(B - V)$	A_K	$(m - M)_0$	$\sigma_{(m - M)_0}$	D (kpc)	σ_D (kpc)
NGC 1651	16.93	0.02	93	-1.56	0.02	0.10	0.034	18.46	0.03	49.1	0.6
SL 61	17.01	0.03	22	-1.52	0.08	0.11	0.038	18.49	0.09	49.9	2.1
NGC 1783	16.93	0.01	384	-1.10	0.18	0.02	0.007	18.02	0.18	40.2	3.4
NGC 1846	16.98	0.01	301	-1.17	0.19	0.06	0.020	18.13	0.19	42.3	3.8
NGC 1978	16.86	0.01	231	-1.56	0.02	0.05	0.017	18.40	0.02	47.9	0.5
Hodge 4	16.81	0.02	48	-1.57	0.02	0.04	0.014	18.37	0.03	47.1	0.6
IC 2146	17.01	0.02	72	-1.56	0.02	0.12	0.041	18.53	0.03	50.8	0.8
SL 663	16.84	0.04	29	-1.52	0.02	0.04	0.014	18.35	0.04	46.7	0.9
NGC 2121	16.83	0.02	184	-1.51	0.02	0.10	0.034	18.31	0.02	45.8	0.5
NGC 2173	16.94	0.03	62	-1.53	0.04	0.10	0.034	18.44	0.04	48.7	1.0
NGC 2155	16.78	0.02	63	-1.53	0.02	0.03	0.010	18.30	0.03	45.7	0.7
NGC 2162	17.10	0.03	72	-1.49	0.18	0.03	0.010	18.58	0.18	52.0	4.5
ESO 121	16.93	0.03	20	-1.20	0.06	0.03	0.010	18.12	0.06	42.1	1.3
NGC 2203	16.97	0.02	128	-1.48	0.16	0.11	0.038	18.41	0.17	48.1	3.8
NGC 2193	16.88	0.04	28	-1.58	0.01	0.04	0.014	18.45	0.04	48.9	0.9
SL 869	17.12	0.06	15	-1.48	0.16	0.10	0.034	18.57	0.17	51.7	4.3
SL 896	16.89	0.07	7	-1.58	0.01	0.09	0.031	18.44	0.07	48.7	1.6

Note. — All numbers are given in magnitudes unless otherwise noted.

Table 5. Effect of LMC Geometry

Geometry (Reference)	R.A. (J2000.0)	Decl. (J2000.0)	Θ (deg)	i (deg)	$(m - M)_0$ (mag)	D_0 (kpc)
van der Marel & Cioni (2001)	5 29 00	-69 30 00	122.5 ± 8.3	34.7 ± 6.2	18.40 ± 0.04	47.9 ± 0.9
Olsen & Salyk (2002)	5 19 38.0	-69 27 05.2	145 ± 4	35.8 ± 2.4	18.41 ± 0.04	48.1 ± 0.9
van der Marel et al. (2002)	5 27 36	-69 52 12	129.9 ± 6.0	34.7 ± 6.2	18.40 ± 0.04	47.9 ± 0.9
Nikolaev et al. (2004)	5 17 36	-69 01 48	151.0 ± 2.4	30.7 ± 1.1	18.41 ± 0.04	48.1 ± 0.9

Note. — Units of right ascension are in hours, minutes, and seconds and units of declination are in degrees, arcminutes, and arcseconds. Distances given are for the LMC center, calculated by combining our cluster distances with the given LMC geometry.

Table 6. LMC Center Distances

Cluster Name	D (mag)	σ_D (mag)	D_0 (mag)	σ_{D_0} (mag)
NGC 1651	18.46	0.03	18.35	0.04
SL 61	18.49	0.09	18.30	0.10
NGC 1783	18.02	0.18	18.05	0.18
NGC 1846	18.13	0.19	18.14	0.19
NGC 1978	18.40	0.02	18.47	0.03
Hodge 4	18.37	0.03	18.47	0.04
IC 2146	18.53	0.03	18.41	0.04
SL 663	18.35	0.04	18.45	0.05
NGC 2121	18.31	0.02	18.28	0.03
NGC 2173	18.44	0.04	18.38	0.05
NGC 2155	18.30	0.03	18.42	0.04
NGC 2162	18.58	0.18	18.73	0.18
ESO 121	18.12	0.06	18.33	0.08
NGC 2203	18.41	0.17	18.29	0.17
NGC 2193	18.45	0.04	18.58	0.05
SL 869	18.57	0.17	18.60	0.17
SL 896	18.44	0.07	18.49	0.07

Table 7. LMC Globular Cluster Information

Cluster (Name)	R.A. (J2000.0)	Decl. (J2000.0)	[Fe/H] (dex)	V_{RR} (mag)	$E(B - V)$ (mag)	D (kpc)
NGC 1466	03 44 33.35	-71 40 17.7	-1.9 ± 0.1	19.33 ± 0.02	0.05	51.8 ± 1.0
Reticulum	04 36 11.00	-58 51 40.0	-1.7 ± 0.1	19.07 ± 0.01	0.00	47.3 ± 1.5
NGC 1841	04 45 23.83	-83 59 49.0	-2.2 ± 0.2	19.31 ± 0.02	0.11	47.6 ± 1.9
NGC 1786	04 59 07.82	-67 44 42.8	-2.3 ± 0.2	19.27 ± 0.03	0.06	50.8 ± 1.6
NGC 1835	05 05 06.58	-69 24 13.9	-1.8 ± 0.2	19.38 ± 0.05	0.09	48.5 ± 2.0
NGC 2210	06 11 31.36	-69 07 17.0	-1.9 ± 0.2	19.12 ± 0.02	0.09	43.5 ± 1.5
NGC 2257	06 30 13.00	-64 19 29.1	-1.8 ± 0.1	19.03 ± 0.02	0.04	44.4 ± 0.8

Note. — Units of right ascension are in hours, minutes, and seconds and units of declination are in degrees, arcminutes, and arcseconds.